AGU PUBLICATIONS

JGR

Journal of Geophysical Research: Biogeosciences

RESEARCH ARTICLE
10.1002/2016JG003668

Special Section:
Atmosphere-ice-ocean-ecosystem processes in a thinner Arctic sea ice regime: the Norwegian young sea ICE cruise 2015 (N-ICE2015)

The seeding of ice algal blooms in Arctic pack ice: The multiyear ice seed repository hypothesis

Lasse M. Olsen[1], Samuel R. Laney[2], Pedro Duarte[1], Hanna M. Kauko[1], Mar Fernández-Méndez[1], Christopher J. Mundy[3], Anja Rösel[1], Amelie Meyer[1], Polona Itkin[1], Lana Cohen[1], Ilka Peeken[4], Agnieszka Tatarek[5], Magdalena Różańska-Pluta[5], Józef Wiktor[5], Torbjørn Taskjelle[6], Alexey K. Pavlov[1], Stephen R. Hudson[1], Mats A. Granskog[1], Haakon Hop[1,7], and Philipp Assmy[1]

[1]Norwegian Polar Institute, Fram Centre, Tromsø, Norway, [2]Biology Department, Woods Hole Oceanographic Institution, Woods Hole, Massachusetts, USA, [3]Centre for Earth Observation Science, University of Manitoba, Winnipeg, Manitoba, Canada, [4]Alfred Wegener Institute Helmholtz Center for Polar and Marine Research, Bremerhaven, Germany, [5]Institute of Oceanology, Polish Academy of Sciences, Sopot, Poland, [6]Department of Physics and Technology, University of Bergen, Bergen, Norway, [7]Department of Arctic and Marine Biology, Faculty of Biosciences, Fisheries and Economics, UiT, Arctic University of Norway, Tromsø, Norway

Key Points:
- Multiyear ice may act as a repository for ice algae during winter
- The repository can seed ice algal blooms in adjacent younger ice during spring
- A shift from a multiyear ice to a first year ice regime in the Arctic might compromise this seeding mechanism

Supporting Information:
- Supporting Information S1

Correspondence to:
L. M. Olsen,
lasse.mork.olsen@npolar.no

Citation:
Olsen, L. M. et al (2017), The seeding of ice algal blooms in Arctic pack ice: The multiyear ice seed repository hypothesis, *J. Geophys. Res. Biogeosci.*, *122*, 1529–1548, doi:10.1002/2016JG003668.

Received 14 OCT 2016
Accepted 21 MAY 2017
Accepted article online 9 JUN 2017
Published online 3 JUL 2017

Abstract During the Norwegian young sea ICE expedition (N-ICE2015) from January to June 2015 the pack ice in the Arctic Ocean north of Svalbard was studied during four drifts between 83° and 80°N. This pack ice consisted of a mix of second year, first year, and young ice. The physical properties and ice algal community composition was investigated in the three different ice types during the winter-spring-summer transition. Our results indicate that algae remaining in sea ice that survived the summer melt season are subsequently trapped in the upper layers of the ice column during winter and may function as an algal seed repository. Once the connectivity in the entire ice column is established, as a result of temperature-driven increase in ice porosity during spring, algae in the upper parts of the ice are able to migrate toward the bottom and initiate the ice algal spring bloom. Furthermore, this algal repository might seed the bloom in younger ice formed in adjacent leads. This mechanism was studied in detail for the dominant ice diatom *Nitzschia frigida*. The proposed seeding mechanism may be compromised due to the disappearance of older ice in the anticipated regime shift toward a seasonally ice-free Arctic Ocean.

Plain Language Summary Ice algae are important primary producers in the Arctic food web. These organisms are adapted to living under extreme conditions in the sea ice environment. It is not well known how ice algae overwinter in the Arctic and are able to bloom the following spring. During the N-ICE campaign R/V *Lance* was frozen into the pack ice north of Svalbard between January and June 2015 and enabled scientists to study the sea ice and the ice algae from winter to summer. We found that multiyear ice because of its characteristic physical structure can function as a seed repository for ice algae and secure a sufficient seed stock for the spring ice algae bloom. During the last decades a change in the ice regime of the Arctic Ocean has been observed where multiyear ice is disappearing fast and ice-free summers could be a reality within this century. This could compromise the seeding mechanism and lead to profound changes in the ice algal species composition and primary productivity.

1. Introduction

Ice algae play a critical role for the ice-associated ecosystem of the Arctic Ocean [*Leu et al.*, 2015]; thus, studying the factors that regulate ice algal blooms will help to improve our understanding of the future role of the ice-associated ecosystem in a rapidly changing Arctic. Ice algae which are adapted to live in the brine channels and pockets inside the sea ice are psychrophiles and halotolerant and can be characterized as extremophiles [*Thomas and Dieckmann*, 2002, *Lyon and Mock*, 2014; *Krembs et al.*, 2002]. Hundreds of algal species can be found in sea ice [*Horner*, 1985; *von Quillfeldt et al.*, 2003; *Poulin et al.*, 2011], but some are more common and tend to dominate in terms of abundance and/or biomass. These species might have special adaptations beyond tolerance for low temperature and high salinity that make them successful in this environment.

Nitzschia frigida, a pennate diatom that forms characteristic arborescent colonies [*Medlin and Hasle*, 1990], often dominates the autotrophic biomass in the bottom or sub-ice assemblage in the Arctic [*Leu et al.*, 2015].

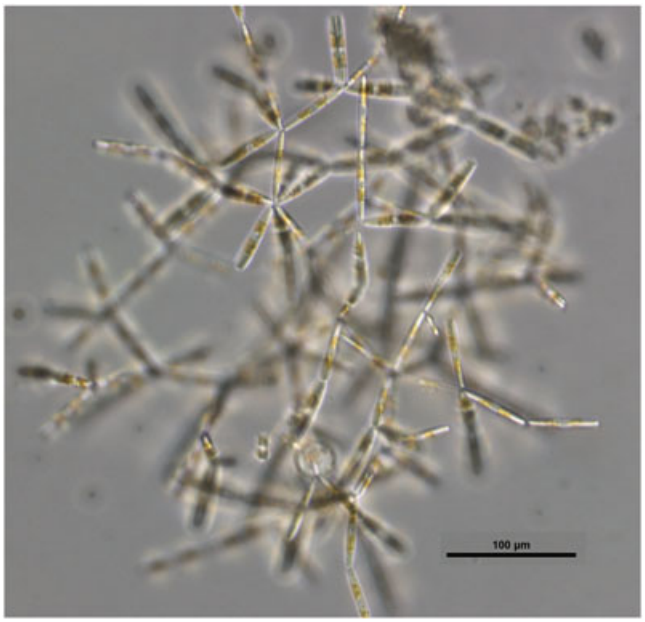

Figure 1. Arborescent colony of *Nitzschia frigida* at 200X magnification. Photo: Philipp Assmy.

The arborescent colony formation (Figure 1) could provide some sort of benefit in the ice environment, e.g., helping anchor algae at the ice water interface. Positioning at the bottom of the ice enables algae immediate access to nutrients from the water column, which is a much larger reservoir than the sea ice itself. *N. frigida* thrives in land-fast first year ice (FYI) [*Syvertsen*, 1991; *Ratkova and Wassman*, 2005], but numerous observations suggest that it is also common in Arctic pack ice [*Leu et al*., 2015]. Laboratory experiments have shown that *N. frigida* tolerates very high brine salinity, can grow at temperatures down to −8°C, and at very low irradiance [*Aletsee and Jahnke*, 1992; *Juhl and Krembs*, 2010]. This species is not known to produce resting spores but may rather survive the extreme winter conditions by simply lowering its metabolism to a minimum [*Aletsee and Jahnke*, 1992; *Zhang et al*., 1995]. During a sub-ice bloom *N. frigida* can be found in the water column, but most studies indicate that it sinks out of the water relatively fast and does not maintain a planktonic population [*Michel et al*., 1993; *Haecky et al*., 1998]. Because the shallow Arctic shelves and the Barents Sea are essentially ice free during summer, ice algae are hypothesized to survive in the sediments and then be brought back to surface waters by deep mixing during the winter [*von Quillfeldt et al*., 2009]. The presence of *N. frigida* in sea ice in areas that are completely ice free in summer such as the Baltic Sea [*Granskog et al*., 2006; *Haecky et al*., 1998] and Hudson Bay [*Michel et al*., 1993] confirms that this mechanism is possible in relatively shallow waters. However, this is unlikely to occur in the deep central Arctic basins where mixing levels are too low to bring up algae from the seafloor to the surface. Therefore, we cannot currently fully explain the dominance of *N. frigida* in sub-ice blooms in Arctic pack ice.

An example of a common ice algae species with a different adaptation to the sea ice is *Fragilariopsis cylindrus*, a pennate diatom that forms ribbon-like colonies [*von Quillfeldt*, 2001], and is commonly found in the Arctic and the Southern Ocean [*Lundholm and Hasle*, 2008]. This species is also adapted to low temperature and high salinity [*Krell et al*. 2008], and it is often found to be dominating in phytoplankton blooms in the marginal ice zone, as well as in areas with no ice. Therefore, *F. cylindrus* could be characterized as cold water adapted and may not strictly need sea ice for survival [*von Quillfeldt*, 2004]. Yet another strategy is employed by *Polarella glacialis*, a cyst-forming dinoflagellate with a bipolar distribution, which is clearly adapted to the changing conditions inside sea ice. It forms resting cysts in the upper part of the ice for overwintering, which excyst in early spring; motile vegetative cells can then move through the brine channels. In late spring and early summer they produce new resting cysts, suggesting that the cysts can be a strategy for both dispersal and overwintering [*Stoecker et al*., 1998; *Montresor et al*., 2003].

The sea ice is a dynamic environment with pronounced changes taking place over the annual cycle. Brine pockets and channels that formed during freezing give sea ice a porous structure. The brine volume fraction is a measure of the porosity of the ice, which increases with increasing temperature [*Golden et al*., 1998, 2007]. In winter, there is a strong temperature gradient in the ice, close to air temperature at the top and near the freezing point of seawater at the bottom. Consequently, the brine volume fraction decreases from bottom to top, and the brine will be increasingly concentrated toward the top, which results in high brine salinity there [*Petrich and Eicken*, 2010]. When the air temperature increases in spring, it warms up the ice, and the gradients in temperature, brine salinity, and porosity eventually weaken and disappear. First year ice (FYI) that survives

the summer melt season will become second year ice (SYI) and, eventually, multiyear ice (MYI) if it survives several summers.

The pack ice (drift ice) of the Arctic Ocean is dynamic and always in motion. In the western Arctic the dominating pattern is a clockwise circulation in the Beaufort Gyre, whereas in the eastern Arctic sea ice is continuously drifting in the direction from the East Siberian Sea and the Laptev Sea across the central Arctic Ocean to the Fram Strait with the Transpolar Drift [*Rigor and Wallace*, 2004]. The pack ice is a mix of FYI, SYI, and MYI, with new ice forming continuously through autumn, winter, and spring as leads open and refreeze [*Willmes and Heinemann*, 2016]. During the last couple of decades, there has been a pronounced reduction of the amount of MYI, and in the near future summers might be ice free in the Arctic Ocean [e.g., *Stroeve et al*., 2012].

Life history adaptations to the dynamic sea ice environment might determine how different ice algae species will respond to the currently ongoing changes in the Arctic sea ice cover, toward a FYI regime. During the Norwegian young sea ICE (N-ICE2015) expedition from January to June 2015, R/V *Lance* was frozen repeatedly into the ice at around 83° north of Svalbard and drifted with the floes to the ice edge [*Granskog et al*., 2016]. This made it possible to study the changes in air, sea ice, and water column properties and the ice algae assemblages during the winter to early summer transition. We followed these changes in FYI, SYI, and young ice (YI). The latter formed in leads during the drift. We studied in particular the development of the dominant sea ice diatom *Nitzschia frigida* in the different ice types, to try to understand how it seeds the pack ice environment.

2. Materials and Methods

2.1. Study Area and Sea Ice Conditions

All samples used in this study were collected during the N-ICE2015 expedition from January to June 2015 in which R/V *Lance* was frozen into the pack ice and drifted with the ice from about 83 to 80°N north of Svalbard, southwestward toward the ice edge with the Transpolar Drift [*Granskog et al*., 2016]. This was repeated four times, and the fourth and last drift was in June near the ice edge (Figure 2). Hereafter, we will refer to the four ice drifts as Floes 1 to 4. The oldest sea ice in the N-ICE2015 region was tracked back in time using a coarse-resolution sea ice drift product from satellite observations (Figure 2) [*Itkin et al*., 2017]. In brief, daily ice motion vectors were calculated from satellite observations with a 3 day time lag. Those vectors were based on advanced scatterometer (ASCAT) and Special Sensor Microwave Imager (SSM/I) radiometer data for the winter months [*Girard-Ardhuin and Ezraty*, 2012]. The summer months were bridged using an unpublished version of summer ASCAT/SSMIS ice drift data by the same provider [*Itkin et al*., 2017]. The ice floes from the region were backtracked to northern Laptev Sea in September 2013. This implies that the oldest sea ice in the N-ICE2015 study area was second year ice (SYI), and the ice pack thus was composed of a mix of first year ice (FYI), second year ice (SYI), and young ice (YI) [e.g., *Granskog et al*., 2017].

Based on the salinity profiles and ice thickness of the ice cores, three sites on Floe 3 (18 April to 5 June) were at the time of sampling identified to be SYI, FYI, and YI, which is also corroborated by the oxygen isotopic composition of the ice [*Granskog et al*., 2017]. Temperature, bulk ice salinity, calculated brine salinity, and brine volume fractions in ice cores from SYI on Floe 3 (Figures 4a–4d) and FYI on Floes 2, 3, and 4 (Figures 4e–4h) indicated that Floe 2 represented winter conditions (early March), while Floe 3 covered the Arctic spring-summer transition (April–May) and Floe 4 the early summer (June). The evolution of YI in a lead that froze during the Floe 3 drift in April was directly observed at five locations along a transect [*Kauko et al*., 2017]. The three different ice types (SYI, FYI, and YI) were repeatedly sampled during the drift to monitor changes during the Arctic winter to summer transition. On Floe 3 the SYI and FYI coring sites were about 100 m apart, and the YI was 300–400 m away from the SYI and FYI sites. Ice core samples from one FYI site in March on Floe 2 and three FYI sites in June on Floe 4 were included to have samples from winter and more into summer. The three sites on Floe 4 were approximately 100 m apart.

2.2. Sample Collection

Ice cores for temperature, salinity and ice structure (stratigraphy) were extracted with a 9 cm ice corer (Mark II coring system, KOVACS enterprise, Roseburg, USA). Ice cores for biological samples were taken with a 14 cm diameter corer (Mark II coring system, KOVACS enterprise, Roseburg, USA), except the cores for biology on the YI, which were extracted with the 9 cm corer. The sites and dates for the sampling of the various ice

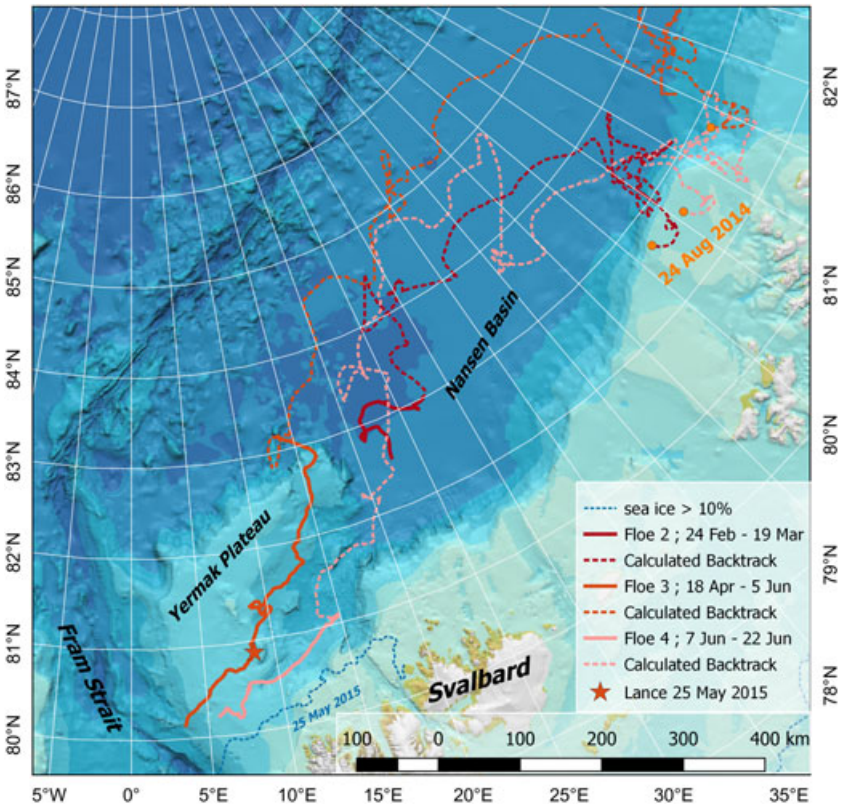

Figure 2. Study area with bathymetry for the N-ICE2015 expedition with R/V *Lance*. The drift trajectories for Floes 2–4 are shown with the start and end dates, and the calculated backtracks to 24 August 2014 for all floes are shown in same color with broken lines. The location of R/V *Lance* on 25 May is indicated with an orange star. The broken blue line indicates the ice edge position on 25 May 2015. Map created at the Norwegian Polar Institute, by Max König. Bathymetry with permission from IBCAO [*Jakobsson et al.*, 2012].

cores are summarized in Table S1. Seawater samples for nutrients, chlorophyll *a*, pigment composition, and algal counts were collected with 8 L Niskin bottles attached to a Sea-Bird rosette water sampler that was equipped with a Sea-Bird Electronics SBE911 conductivity temperature and pressure sonde (CTD). Water samples for algal counts were taken at 5, 25, and 50 m depths (Table S1). In addition, 24 L of seawater were concentrated to 90 mL by gently filtering through 10 μm gauze to collect rare microplankton species. Ice-tethered sediment traps were deployed in two ways: at 1 m below the ice attached to a rope deployed by divers under the ice and at 5, 25, 50, and 100 m depths along a mooring attached to the ice (Table S1). The deployment time varied between 36 and 72 h but was usually close to 48 h. The trap cylinders were filled with a saturated NaCl solution to avoid sample loss from the traps during deployment and recovery. Swimmers (copepods and other zooplankton) were removed before subsampling for algal taxonomy. The sinking flux for ice algae cells was calculated from the cell concentration in the traps, the volume and area of the traps, and the deployment time.

2.3. Environmental Conditions

Air temperature was measured with Vaisala HMP155 sensors mounted inside triple-walled actively aspirated radiation shields (RM Young Model 43502), as a part of the weather observations [*Hudson et al.*, 2015; *Cohen et al.*, 2017]. The sensor was mounted 2 m above the snow surface. Seawater temperature at 2 m below the ice was measured during daily casts with CTD and MSS-90 microstructure profiler [*Meyer et al.*, 2017].

Downwelling solar photosynthetically active radiation (PAR, 400–700 nm) above the ice surface as well as under SYI on Floe 3 and under FYI on Floe 4 was continuously measured with an upward looking cosine-corrected Ramses spectroradiometer (Ramses ACC, Trios GmbH, Germany) [*Taskjelle et al.*, 2016]. Irradiance in the PAR spectrum under FYI and YI on Floe 3 was calculated from the measured surface irradiance using light extinction coefficients for ice and snow from *Light et al.* [2008] in the case of FYI and with measured

ones for the YI [*Kauko et al*., 2017]. The initial conditions used for irradiance calculations under SYI on Floe 3 were snow depth 40 cm and ice thickness 130 cm and for FYI on Floe 3 snow depth 20 cm and ice thickness 120 cm, and for YI on Floe 3 the average conditions were snow depth 3.5 cm and ice thickness 23.8 cm [*Kauko et al*., 2017]. For FYI on Floe 4 snow depth was 20 cm and ice thickness 120 cm. The rate of change of snow and ice thickness on FYI and SYI on Floe 3 (Figure 2) measured by electromagnetic inductive soundings between 27 April and 4 June was −3 and −6 cm per 30 days, respectively [*Rösel et al*., 2016]. With such small changes using constant snow and ice thickness in the irradiance calculations for FYI induce only a minor error in the calculated irradiance at the bottom of the ice. For the YI with maximum 6 cm of snow such a change can alter the irradiance transmission considerably, but our calculations assuming constant 3.5 cm snow depth corresponded well with point measurements of the average daytime irradiance with maximum around 150 μmol photons m^{-2} s^{-1} [*Kauko et al*., 2017].

Water samples for the inorganic nutrients nitrate and nitrite (NO_3 + NO_2), phosphate (PO_4), and silicic acid ($SiOH_4$) were collected 5 m below the ice, fixed with 0.2 mL chloroform and stored refrigerated until sample analysis approximately 6 months later. Nitrate, nitrite, phosphate, and silicic acid were measured spectrophotometrically at 540, 540, 810, and 810 nm, respectively, on a modified scalar autoanalyzer.

For salinity measurements, the total length of the cores was measured before they were cut with a stainless steel saw in 10 cm sections. Bulk ice salinity was measured from the melted samples with a WTW Cond 3110 probe (WTW Wissenschaftlich-Technische Werkstätten GmbH, Weilheim, Germany). Additional cores from the same location on the ice floes were taken for temperature, stratigraphy, oxygen isotope, and nutrient measurements [*Gerland et al*., 2017; *Granskog et al*., 2017]. Brine salinity and brine volume fraction in the ice were calculated based on the measured temperature and bulk salinity according to the equations in *Cox and Weeks* [1986]. Because density was not measured, the air volume fraction needed to calculate the brine volume fraction (porosity) was calculated with the sea ice density set to 0.9 kg dm^{-3} [*Timco and Frederking*, 1996]. Nutrient samples were taken from ice core sections melted in gas-tight bags and analyzed according to the method described above for water samples.

Sea ice texture was examined in dedicated cores [cf. *Granskog et al*., 2017]. In the cold lab (−20°C) at the Norwegian Polar Institute, the cores were cut into approximately 10 cm sections, which were subsequently cut lengthwise into flat square pieces with a thickness of about 1 cm. These pieces were attached to a glass plate by freezing with water for adhesion, and then a microtome (Leica) was used to make a smooth surface. First, thick sections with a thickness of 5–7 mm were prepared and images were taken of the structure of the ice with air pockets, brine channels, and other features. Then the microtome was used to make thin sections with a thickness of <1 mm. These were viewed under cross-polarized light to visualize the ice crystal structure, and digital images were recorded. The thick and thin sections were used to characterize the ice structure throughout the cores, to deduce the structure of the ice [e.g., *Sinha*, 1977; *Lange*, 1988; *Granskog et al*., 2017].

2.4. Algal Taxonomy, Abundance, and Pigments

The ice cores for ice algal samples were cut into 10 or 20 cm sections then put in cleaned opaque plastic containers with lids and subsequently melted overnight at room temperature on board the ship according to *Rintala et al*. [2014]. From the melted volume 190 mL subsamples were filled into 200 mL brown glass bottles and were fixed with 25% glutaraldehyde and 20% hexamethylenetetramine-buffered formaldehyde at a final concentration of 0.1% and 1% (vol/vol), respectively. Water samples for phytoplankton were fixed in the same way, and the concentrated microplankton samples were fixed with 20% hexamine-buffered formaldehyde at a final concentration of 2%. All plankton samples were stored dark and cool.

Algae in the nanosize and microsize fraction were counted from digital micrographs collected with a variant of the Imaging Flow Cytobot (IFCB), as described by *Laney and Sosik* [2014]. Analysis was performed after the cruise on preserved samples. Consequently, cell images were collected by triggering the IFCB to particle scattering and not chlorophyll fluorescence as is usually done [*Olson and Sosik*, 2007]. Five milliliters of the sample was injected through an 860 × 180 μm flow cell through which a 635 nm laser beam was focused. Laser light-scattered off particles in the flow were detected by a photomultiplier tube and triggered the acquisition of a digital micrograph of that particular cell, chain, or colony. A Nitex screen with nominal mesh size of 130 μm was placed on the instrument's sample intake to prevent larger particles from clogging the flow cell. Because of the necessity of using particle scatter instead of fluorescence to trigger images, a higher proportion of

images contained detritus and other nonalgal particulates. Images of algae were discriminated from these manually, using custom software written by one of the authors (S. R. L.).

Assessment of the abundance of ice algae in the water column and sediment traps and a more thorough study of three ice samples for species ID benchmarking was performed by microscopy. For microscopy counts, samples were settled in 50 mL Utermöhl sedimentation chambers (HYDRO-BIOS©, Kiel, Germany) for 48 h. The algae were counted and identified in an inverted Nikon Ti-U light microscope using the Utermöhl method. Cell counts were performed on parallel transects. A minimum of 50 cells of the dominant species were counted in each sample (i.e., maximum error of ±28% according to *Edler and Elbrächter* [2010]).

Samples for chlorophyll *a* (Chl *a*) were collected on 25 mm GF/F filters (Whatman). The volume filtered was noted. Chlorophyll *a* was extracted on the ship in 100% methanol for 12 h at 5°C and measured fluorometrically using a Turner Fluorometer 10-AU (Turner Design, Inc.). Phaeopigments were measured by fluorescence after acidification with 5% HCl [*Holm-Hansen and Riemann*, 1978]. One sample set from early June on Floe 3 was accidentally not stirred before resampling for counts in the IFCB, and therefore, an artificially high Chl *a* per cell ratio was obtained. These samples were not included in the further analysis.

Samples to measure algal pigment composition were taken to derive information about the physiological status of the cells in two cores from SYI from 22 April and 21 May. Pigments were measured using a Waters 1525 binary pump equipped with an autosampler (OPTIMAS™), a Waters photodiode array detector (2996), a Waters fluorescence detector (2475), and the EMPOWER software. Pigments were analyzed by reverse-phase high-performance liquid chromatography (HPLC) using a VARIAN Microsorb-MV3 C8 column (4.6 × 100 mm) and HPLC-grade solvents (Merck). For further details see *Tran et al*. [2013].

To test if the variation in the algal composition was higher between sampling days than between replicate samples, i.e., temporal versus spatial variation, we used the Analysis of Similarity (ANOSIM) test. From the abundance of the algal groups, the Bray-Curtis dissimilarity between samples was calculated. ANOSIM compares ranks of dissimilarities between and within groups and compares the means, with R statistics of 1 for total separation and 0 for no separation [*Clarke*, 1993]. Statistical analysis was performed with packages in the R 2.7.1 platform [*R Development Core Team*, 2008].

3. Results

3.1. Environmental Setting

Floe 2 drifted from 24 February to 19 March at 83–82°N over the Nansen Basin with bottom depth >3000 m. Floe 3 drifted from 18 April to 5 June in a southwestward direction from 83 to 80°N initially over the Nansen Basin but for the most part over the eastern side of the Yermak Plateau, with bottom depth >1000 m until late May, which thereafter gradually shallowed to 500 m until early June. Floe 4 drifted near the ice edge from 7 to 22 June between 81 and 80°N where the depth gradually decreased from 2000 to 500 m (Figure 2).

Data sets that are not further cited in the text are from *Assmy et al*. [2016], *Assmy et al*. [2017], and *Olsen et al*. [2017]. SYI and FYI on Floe 3 had a similar thickness of about 1.2–1.3 m, typically with 40–50 cm, and around 20 cm of snow on top for the two ice types, respectively [*Rösel et al*., 2016]. The SYI had a 50 cm thick layer of granular ice in the top, partly being snow-ice or superimposed ice [*Granskog et al*., 2017], whereas the granular layer was about 15–20 cm thick in the FYI and was partly snow-ice [*Granskog et al*., 2017]. Below the granular ice there was columnar ice down to the bottom in both ice types. No colored layers with algae or sediments were visible by eye, except a light brown coloration of the bottom part during the peak of the ice algal bloom. The YI grew to a thickness of approximately 25 cm from 1 to 20 May during drift of Floe 3 and at the five sites studied had a 4–17 cm thick layer of granular ice, representative of consolidated frazil ice, at the top and columnar ice below. The snow thickness varied between 2 and 6 cm with an average of 3.5 cm during the drift [*Kauko et al*., 2017]. The measured downwelling irradiance immediately under SYI from late April to early June (Floe 3) was 0.1–1 μmol photons m^{-2} s^{-1}, and according to our calculations, it was 1–20 and 10–150 μmol photons m^{-2} s^{-1} under FYI and YI, respectively. All ice cores collected on Floe 4 were FYI [*Granskog et al*., 2017], and the measured transmitted irradiance was 1–20 μmol photons m^{-2} s^{-1} (Figure 3a).

The winter to early summer transition with a steady increase in air temperature from −20 up to around 0°C from April to June, seen on Floe 3 [*Hudson et al*., 2015; *Cohen et al*., 2017], is a typical development for the high

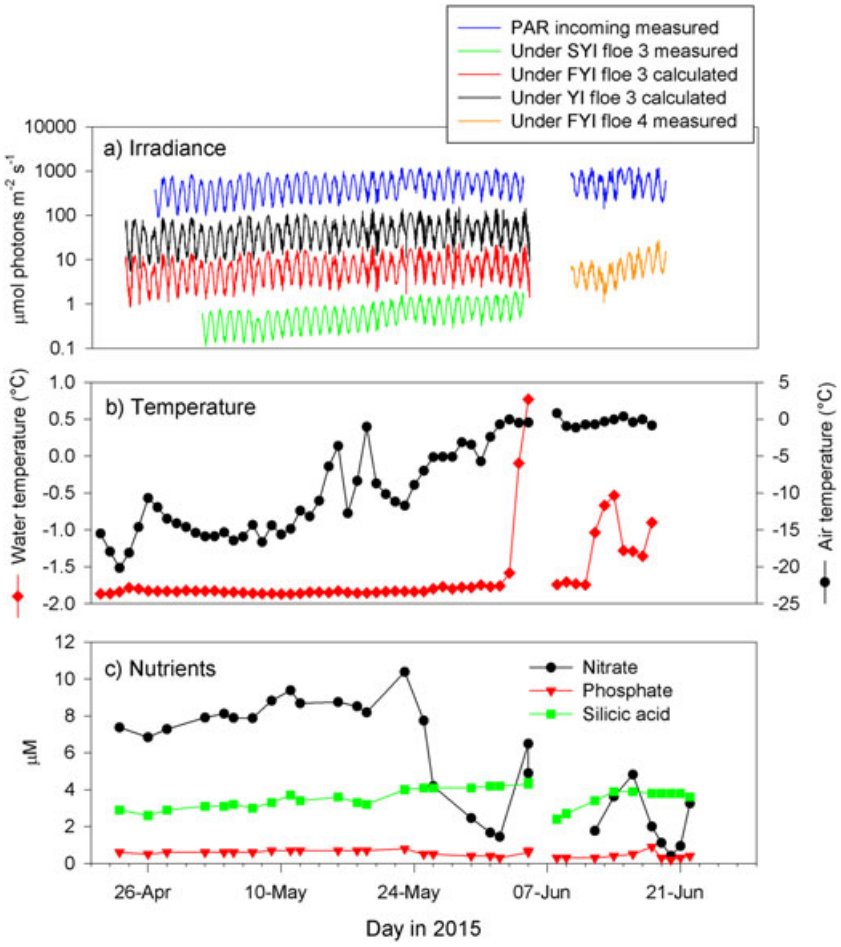

Figure 3. Environmental setting during the drifts of Floes 3 and 4. (a) Irradiance (µmol photons m^{-2} s^{-1}) in the wavelength interval 400–700 nm, i.e., photosynthetically active radiation (PAR), incoming measured at the ice surface, transmitted measured under SYI on Floe 3 and under FYI on Floe 4 [*Taskjelle et al*., 2016], and calculated under YI and FYI during the drift of Floe 4. The data gap is due to the repositioning to Floe 4. (b) Temperature (°C) in the air [*Hudson et al*., 2015] and in the under-ice water at 2 m depth and (c) concentration (µ*M*) of nitrate, phosphate, and silicic acid in the under-ice water at 5 m depth.

Arctic [*Rigor et al*., 2000]. Water temperature immediately below the ice was close to −1.8°C, i.e., freezing temperature for seawater with salinity of around 35, characteristic of Polar Surface Water (PSW) [*Meyer et al*., 2017]. The very rapid increase in water temperature up to 0.8°C in just 3 days from 2 to 5 June (Figure 3b) occurred because Floe 3 drifted over warm Atlantic water [*Meyer et al*., 2017]. Floe 4 initially drifted over PSW with temperature at the freezing point, but after 11 June, the floe entered warmer Atlantic water again with temperature varying between −1.3 and −0.5°C (Figure 3b).

The ice temperature gradient was most pronounced during winter and early spring with a temperature near the top of the ice of −7.4°C in the SYI on 22 April (Figure 4a) and −6.4°C near the top of the FYI on 5 March (Figure 4e). As the air temperature increased (Figure 3b), this gradient gradually decreased in both ice types until June when the ice became isothermal at the seawater freezing temperature (Figures 4a and 4e). The highest brine salinity (120) was in the top of the SYI on 22 April (Figure 4c) and 105 in the top of the FYI on 5 March (Figure 4g). As the ice temperature increased, the brine salinity decreased gradually in both ice types until it was below seawater salinity throughout the ice in June (Figures 4c and 4g).

The calculated brine volume fraction in the SYI profiles showed a gradient with 15–20% at the bottom and close to 0% at the top. It did not show a clear trend over time, except that the brine volume fraction was higher throughout the entire profile on 4 June (Figure 4e). In FYI, the profiles showed higher volume

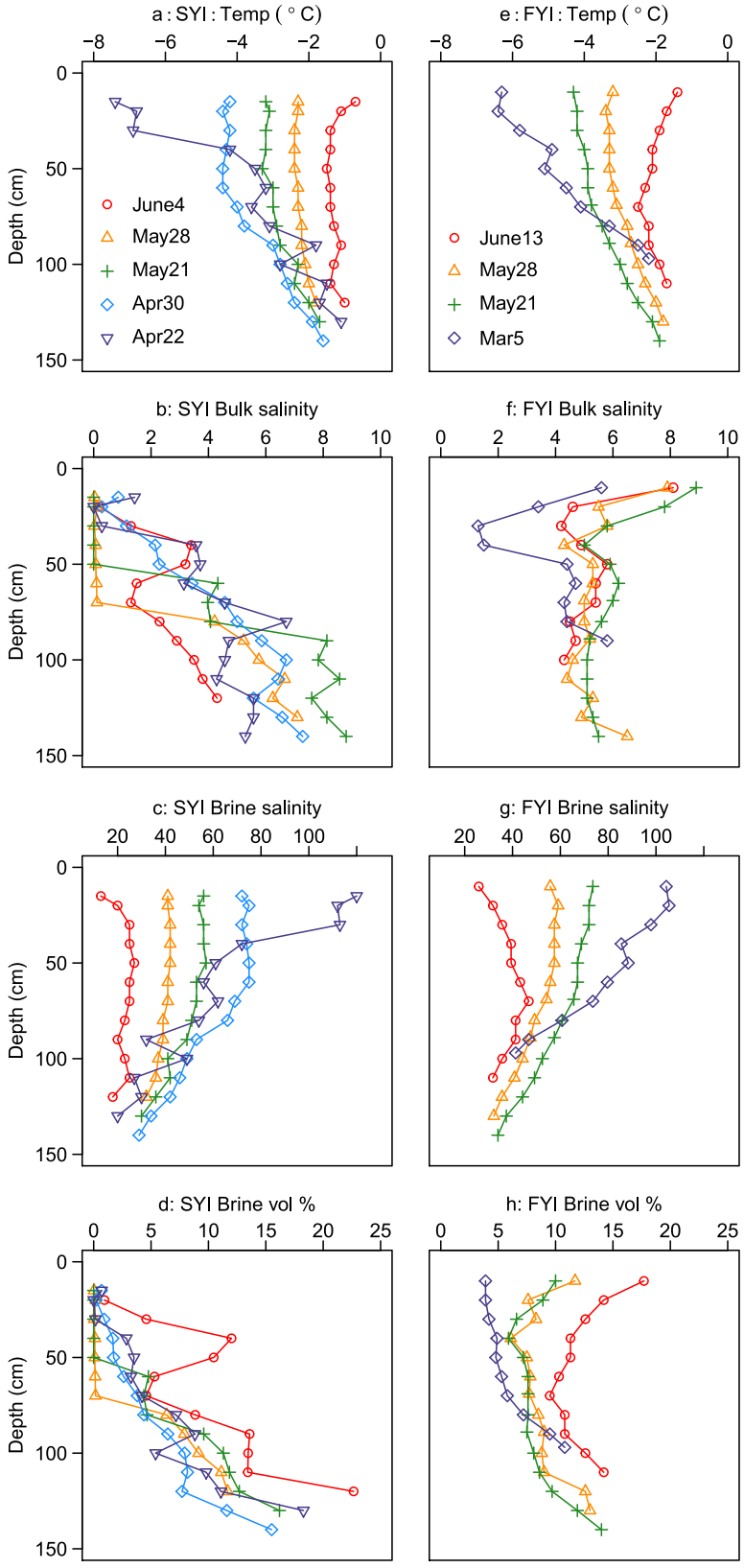

Figure 4. (a and e) Measured ice temperature (°C), (b and f) measured bulk salinity, (c and g) calculated brine salinity, and (d and h) calculated brine volume fraction in depth profiles of MYI (Figures 4a–4d) and FYI (Figures 4e–4h). For MYI the time series is from 22 April to 4 June (Floe 3) and for FYI from 5 March to 13 June (Floes 2, 3, and 4).

fractions both in the core bottom and tops than in SYI (Figure 4h). In the FYI core from Floe 2 in March, the volume fraction was 4–5% in the upper part and increased to 11% in the bottom part (Figure 4h). All later FYI cores had volume fractions >5% throughout the cores. In the FYI core from Floe 4 in June, the volume fraction was 9–18% (Figure 4h).

The phosphate concentration below the ice at 5 m depth was stable at around 0.6 μM from 7 May to 3 June (Figure 3c). Silicic acid was also relatively stable (3–4 μM), whereas the nitrate concentration was close to 9 μM until 24 May, increased thereafter to about 11 μM for a few days, and then quickly declined to <2 μM after 5 June (Figure 3c). In the melted ice cores the silicic acid concentration was always below the detection limit of 0.7 μM, in both SYI and FYI (not shown). On 22 April the nitrate concentration was between 0.5 and 2 μM through the SYI core, except the higher value of 17 μM at the very top. On 28 May the concentration was reduced to below the detection limit of 0.4 μM in the upper ice core but remained just above the detection limit at the bottom (Figure S1 in the supporting information). In the FYI, the nitrate concentration was around 0.5 μM through the ice core on 5 March, and below the detection limit through the core on 28 May, except a value just over the detection limit at the bottom (Figure S2). The phosphate concentration remained in the range 0.05–0.2 μM throughout both FYI and SYI cores from March/April to May (Figures S3 and S4).

3.2. Algal Abundance and Pigment Concentration in the Ice

3.2.1. Second Year Ice

The IFCB imagery revealed that ice algal abundance in SYI on Floe 3 in April and early May peaked at 150–200 $\times 10^3$ cells L^{-1} in the upper part between 20 and 80 cm below the surface (Figures 5a–5d). In this layer, 50–90% of the identified cells were pennate diatoms, while the remainder were primarily resting cells, recognized by shape and by being optically dense compared with vegetative cells. Low abundance of centric diatoms (e.g., *Thalassiosira* sp.) and ciliates was observed. The pennate diatoms found in the upper ice maximum were mainly of a shape resembling *N. frigida*, but always as single cells and therefore not easy to determine given the resolution of the IFCB imagery. Microscopy investigation of the upper abundance maximum of SYI cores from 22 April and 14 and 21 May confirmed the dominance of pennate diatoms with *N. frigida* being the main contributor, whereas resting cells, flagellates, centric diatoms, and ciliates accounted for the remainder of the assemblage (Figure S5). The resting cells were a mix of chrysophyte and dinoflagellate cysts, and the flagellates were a mix of mostly unidentified species <10 μm, and *Phaeocystis* in the sample from 21 May. At the bottom part of the ice, some colonial *N. frigida* were identified from IFCB images in the samples from 22 April and 14 May (Figures 5a and 5b). An increase in algal abundance was seen at the bottom of the ice on 21 and 28 May (Figures 5c and 5d), dominated by the pennate diatom *Nitzschia frigida* as recognized by its distinctive arborescent colonies [*Medlin and Hasle*, 1990]. Overall, the Chl *a* profiles were correlated with cell count profiles (Pearson correlation $r = 0.61$, $p < 0.01$, $n = 31$) with some exceptions (Figures 5a–5d). The mean Chl *a* per cell ratio in the core samples from all depths from April and May was in the range of 1.9 to 4.6 $\times 10^{-11}$ g per cell, with tendency of increasing ratio toward the bottom of the cores.

Chl *a* and *b* degradation products were only occasionally detected in some sea ice sections. The concentrations of phaeophythin *a*, indicative of senescence [*Owens and Falkowski*, 1982], were higher on 21 May than on 22 April, and phaeophorbide *a*, indicative of grazing [*Head and Harris*, 1992], was only detected on 21 May (Figure S6, first group, GR1). These pigments were all detected in only one ice core segment; i.e., they were rare in the ice. Diagnostic marker pigments reveal some variations between the two cores, which was mainly governed by changes of some flagellate groups (Figure S6, second group, GR2). When looking at the marker pigments, the high fucoxanthin/Chl *a* ratio followed by the less specific chlorophyll c12/Chl *a* ratio supports the microscopic and IFCB observations of the dominance of diatoms in the sea ice. Overall, the ratios are not significantly different between the two sampling dates and indicate a dominance of diatoms already in April. Another algae group identified in the sea ice cores belonged to chlorophytes, which are presented by chlorophyll *b*, violaxanthin, neoxanthin, and lutein ratios, which also showed similar ratios in both sea ice cores. The 19-butanoyloxyfucoxanthin, which was only present in April, is indicative for pelagophytes, while autotrophic dinoflagellates, indicated by the presence of peridinin, occurred only in May. Chlorophyll C3 to chlorophyll *a* strongly increased in May and must be considered as a strong indicator for the presence of *Phaeocystis* sp. [*Jeffrey and Vesk*, 1997; *Fragoso et al*., 2016].

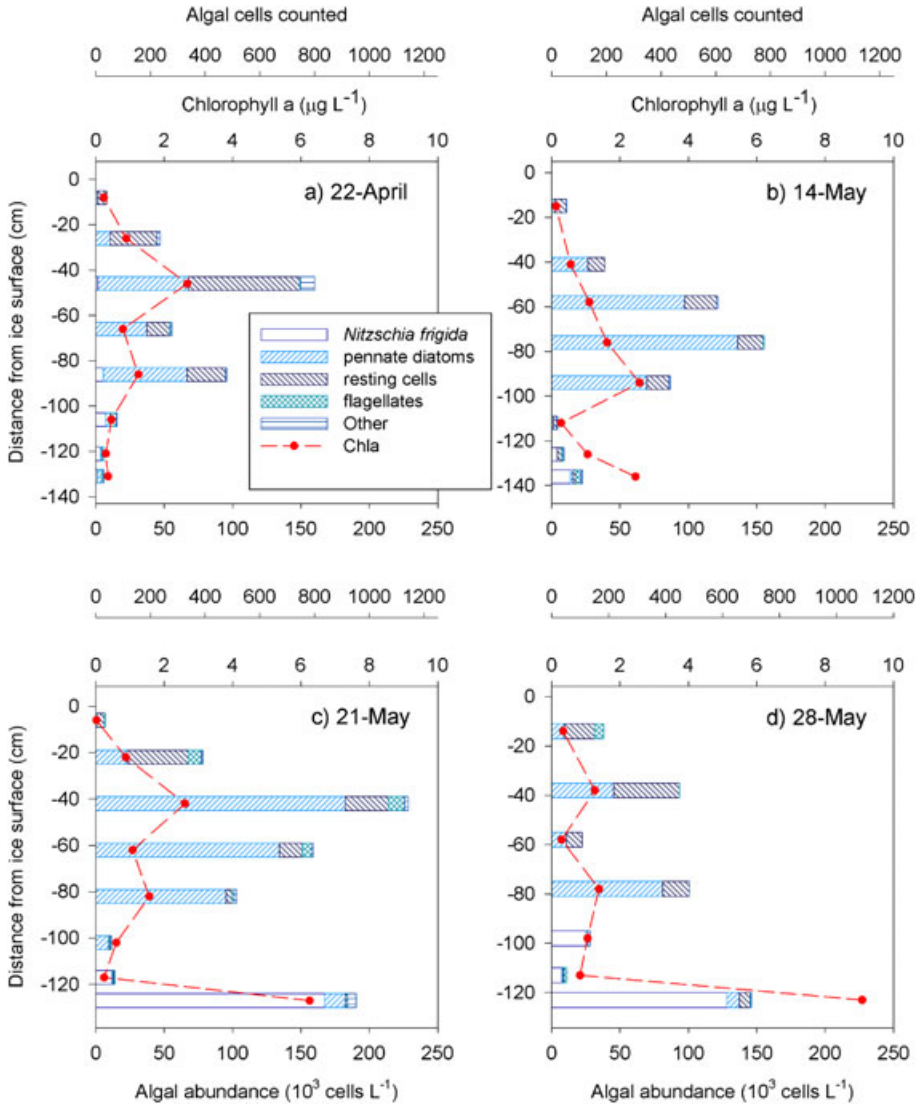

Figure 5. Counts of algae (10^3 cells L^{-1}) by Imaging Flow Cytobot (IFCB) in a time series of depth profiles in ice cores from SYI on Floes 3 and 4, from 22 April to 28 May. The algae were categorized as *Nitzschia frigida*, other pennate diatoms, resting spores, flagellates, and other, which includes centric diatoms and ciliates. The ice depths indicated on the *y* axis are the middle value of the depth interval for the different parts of the ice cores from which the samples were taken. The red circles indicate the average chlorophyll *a* concentration (μg L^{-1}) on the first upper *x* axis. The uppermost *x* axis indicates the number of algal cells counted denoted by the bars. A large fraction of the pennate diatoms in the upper ice was *N. frigida* (see Figure S5).

3.2.2. First Year Ice

The IFCB imagery from FYI core from 12 March on Floe 2 indicated a dominance of resting spores (60–90%) with the remaining cells mainly pennate diatoms (Figure 6a). These diatoms were single celled and resembled the cells observed in the upper part of SYI, which were identified to be mainly *N. frigida*. Abundance maximum was observed 30 cm below the ice surface in March, although the cell counts ($2–35 \times 10^3$ cells L^{-1}) were considerably lower than in the upper maximum in SYI. The FYI cores on Floe 3 did not have an upper ice maximum at all with $<10 \times 10^3$ L^{-1} throughout the ice (Figures 6b–6d). A bloom developed at the bottom of the ice during May with a peak abundance of ~150×10^3 cells L^{-1}, similar to the development of the bottom bloom in SYI (Figure 5). Resting spores and pennate diatoms were the dominating groups on 14 May, with an increased abundance of diatoms at the bottom of the core (Figure 6b). Most pennate diatoms were single cells with shape resembling *N. frigida*, and in the bloom 70–90% of the cells were identified to be *N. frigida* (Figures 6c and 6d). The abundance profiles were different in the FYI cores from Floe 4, which had *N. frigida* in colonial form all through the ice with abundance up to 100×10^3 cells L^{-1}

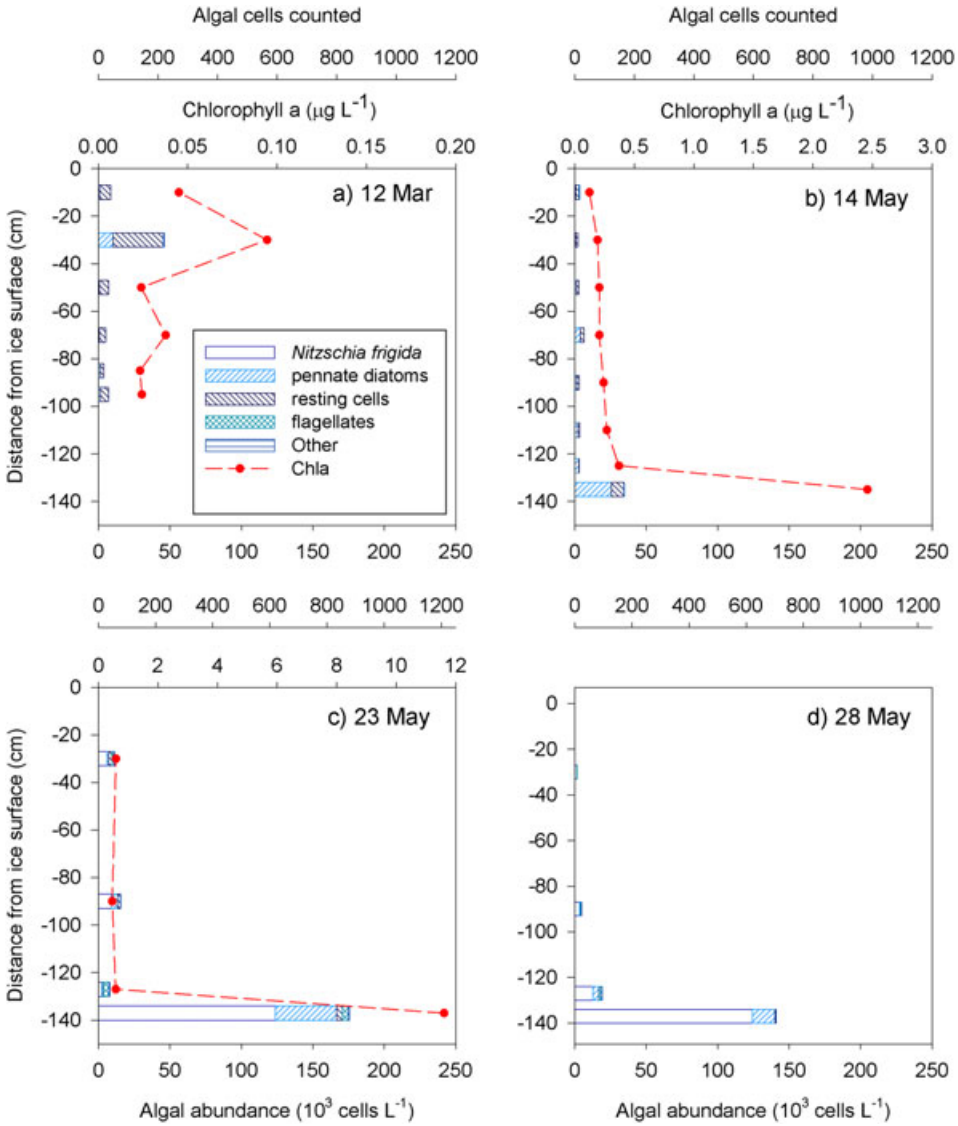

Figure 6. Counts of algae (10^3 cells L^{-1}) by Imaging Flow Cytobot (IFCB) in a time series of depth profiles in ice cores from FYI on Floes 2 and 3, from 12 March to 28 May. The algae were categorized as *Nitzschia frigida*, other pennate diatoms, resting spores, flagellates, and other, which includes centric diatoms and ciliates. The ice depths indicated on the *y* axis are the middle value of the depth interval for the different parts of the ice cores from which the samples were taken. The red circles indicate the average chlorophyll *a* concentration (μg L^{-1}) on the first upper *x* axis. The uppermost *x* axis indicates the number of algal cells counted denoted by the bars.

in the upper ice (Figures 7a–7c). On site 1 we observed a maximum abundance at the bottom like the cores from 23 and 28 May on Floe 3 (Figures 7a, 6c, and 6d). In the cores from sites 2 and 3 there was no maximum at the bottom (Figures 7b and 6c). In general, half or more of the algae were pennate diatoms and mainly *N. frigida* throughout the cores. The remaining algae were flagellates and resting cells, mainly *Polarella glacialis* resting cysts (Figures 7a–7c). A correlation analysis between Chl *a* and cell counts for all FYI cores from Floes 3 and 4 gave Pearson $r = 0.91$ and $p < 0.01$ with $n = 33$.

3.2.3. Young Ice

Initially, the YI of the refrozen lead was dominated by cryptophyte chloroplasts that presumably originated from burst cells of the kleptoplastidic ciliate *Mesodinium rubrum* which appeared under the thin ice in early May. On 14 May a few of these cryptophyte chloroplasts still remained together with other flagellates and centric diatoms in low abundance (Figure 8a). Flagellates and centric diatoms still dominated on 22 May, but *Nitzschia frigida* and other pennate diatoms had started to appear, especially in the core bottom

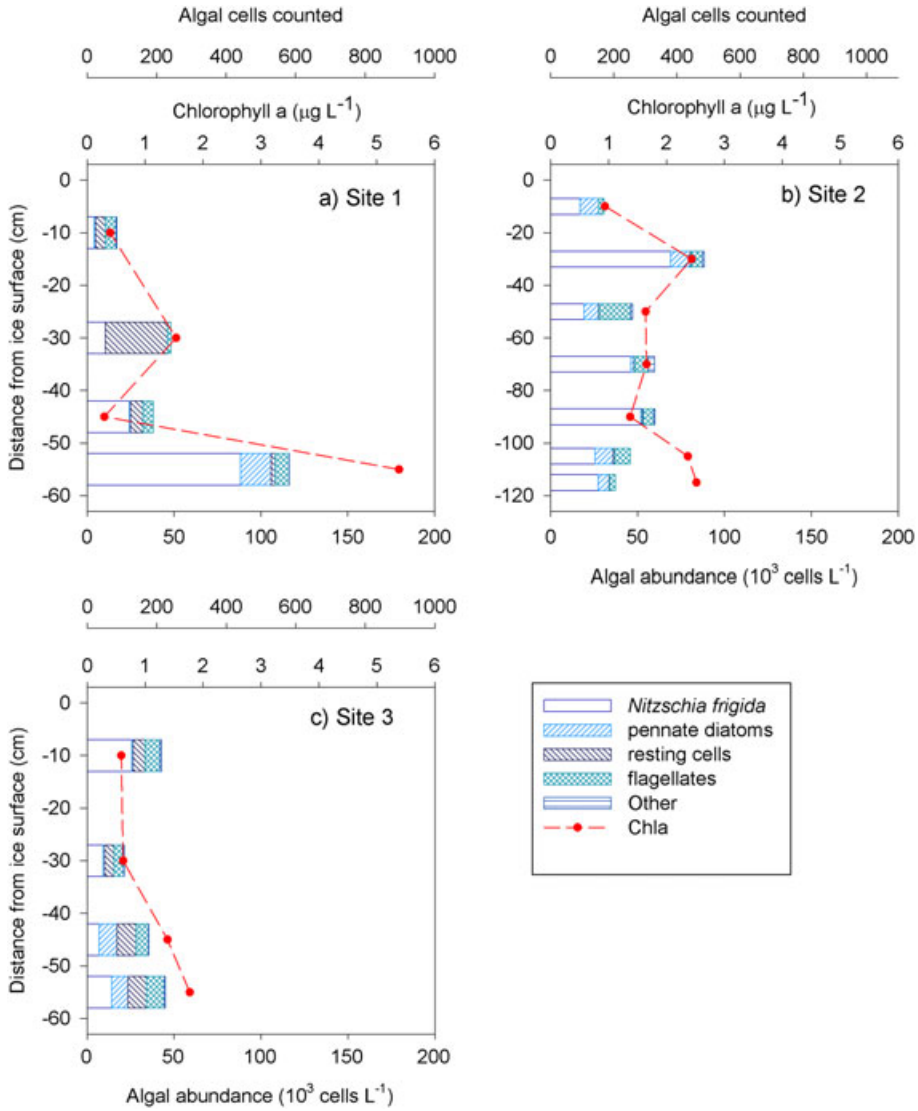

Figure 7. Counts of algae (10^3 cells L^{-1}) by Imaging Flow Cytobot (IFCB) in depth profiles from three ice cores from 3 FYI sites on Floe 4 in June. The algae were categorized as *Nitzschia frigida*, other pennate diatoms, resting spores, flagellates, and other, which includes centric diatoms and ciliates. The ice depths indicated on the *y* axis are the middle value of the depth interval for the different parts of the ice cores from which the samples were taken. The red circles indicate the average chlorophyll *a* concentration (μg L^{-1}) on the first upper *x* axis. The uppermost *x* axis indicates the number of algal cells counted denoted by the bars.

sections. Some resting cysts were also present at this time (Figure 8b). On 29 May, pennate diatoms were dominating in the core bottoms forming a typical bottom interstitial assemblage (Figure 8c). Arborescent colonies of *N. frigida* dominated, while *Navicula* spp. constituted the bulk of the remaining pennate diatoms. At this time, resting cysts were present at higher abundances than previously seen and were particularly numerous with up to 30% of the total cell numbers in the core tops (Figure 8c). These were mainly cysts of the phototrophic dinoflagellate *Polarella glacialis*. The ANOSIM test based on the Bray-Curtis similarity of the algal communities between the five sites on the YI and between sampling days 22 and 29 May yielded an R value between 0.71 and 1 and $p < 0.013$ for all tests of bottom versus bottom, top versus top, and top versus bottom of ice cores. The Chl *a* profile matched the counts well on all sampling dates (Figure 8d), and there was a good correlation (Pearson $r = 0.96$, $p < 0.01$, $n = 25$).

3.2.4. Abundance of *N. frigida* in the Water Column

The microscopy counts from the 10 μm concentrated water samples indicated a *N. frigida* abundance of <6 cells L^{-1} throughout the winter (Table 1). The first appearance of *N. frigida* cells in the under-ice

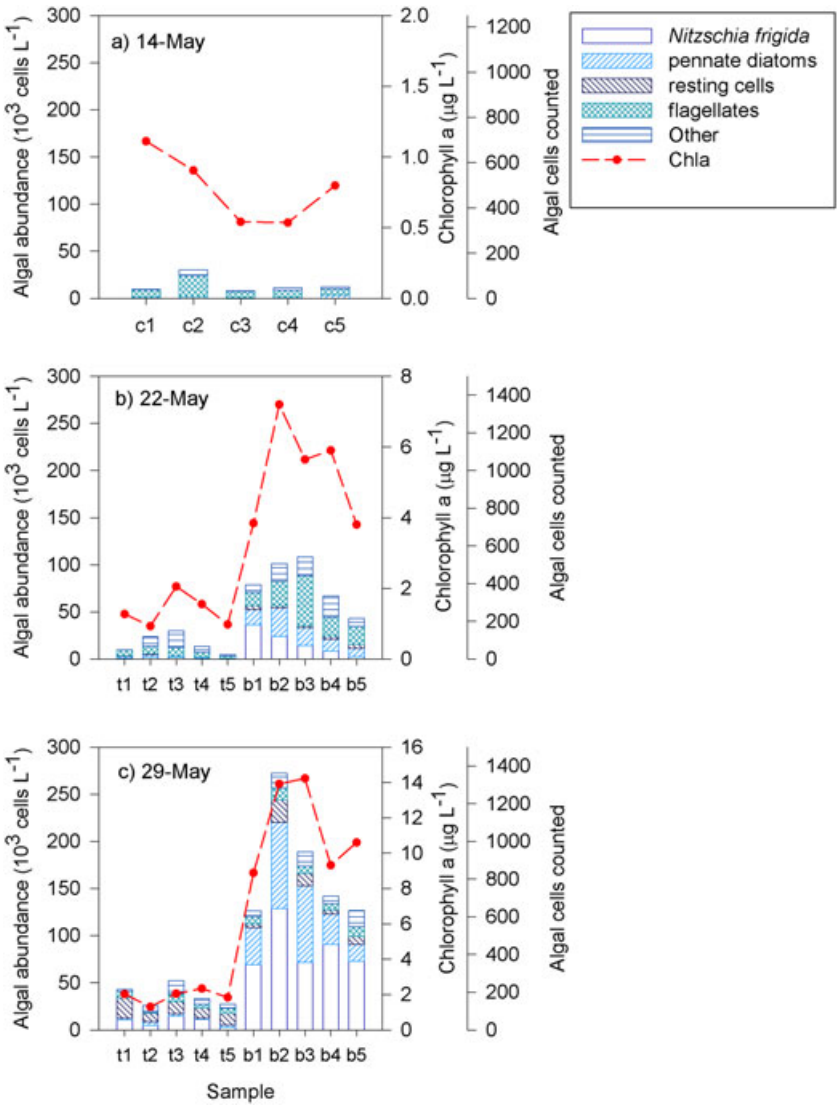

Figure 8. Counts of algae (10^3 cells L^{-1}) by Imaging Flow Cytobot (IFCB) in top and bottom parts of YI cores on Floe 3 from 14 to 28 May taken in a transect with five cores. On 14 May the top and bottom parts were pooled and whole cores are denoted c1–c5. From 14 and 28 May counts from bottom 10 cm of the cores (b1–b5) are presented, and the rest of the core above as top (t1–t5). The algae were categorized as *Nitzschia frigida*, other pennate diatoms, resting spores, flagellates, and other, which includes centric diatoms and ciliates. The red circles indicate the average chlorophyll *a* concentration (μg L^{-1}) on the first *x* axis to the right. The rightmost *x* axis indicates the number of algal cells counted denoted by the bars.

sediment traps was on 8 May (Table 1). In the traps at 1 m depth, the calculated sinking flux increased on 15 May by 1 order of magnitude to around 20×10^3 cells m^{-2} d^{-1} and further to 115–899×10^3 cells m^{-2} d^{-1} on 29 May (Table 1). On 12 June, the sinking flux was 59–314×10^3 cells m^{-2} d^{-1} (Table 1).

4. Discussion

4.1. *Nitzschia frigida* Overwintering in the Upper Part of Multiyear Ice

The most conspicuous feature of the SYI on Floe 3 was the maximum abundance of ice algae in a layer in the upper part of the ice, which consisted of mainly *N. frigida*, other pennate diatoms, various resting cells, and flagellates. FYI did not have this upper maximum, except for a much less pronounced one in early March. The algae did not form a visible band in the ice and therefore can be characterized as a brine channel assemblage, according to *Syvertsen* [1991]. The distribution of algae in the upper part of SYI was not confined to a

Table 1. Abundance of *Nitzschia frigida* (Cells L^{-1}) in Seawater and Sediment Trap Samples and Calculated Sinking Flux (10^3 cells m^{-2} d^{-1}) From Floes 1–4, January to June 2015; *n* Is Number of Cells Detected, and Errors Denote the Precision of Counts Based On *n* [*Edler and Elbrächter*, 2010][a]

Floe	Date	Source	Depth (m)	*n*	Cells L^{-1}	Flux (10^3 Cells m^{-2} d^{-1})
1	26 Jan	Water	5	0	0.0	
1	26 Jan	Water	25	2	1.5 ± 2.1	
1	26 Jan	Water	50	8	6.0 ± 4.2	
1	9 Feb	Water	5	5	3.7 ± 3.3	
1	9 Feb	Water	25	1	0.8 ± 1.6	
1	9 Feb	Water	50	0	0.0	
2	9 Mar	Water	5	7	5.2 ± 3.9	
2	9 Mar	Water	25	0	0.0	
2	9 Mar	Water	50	0	0.0	
3	21 Apr	Water	5	2	1.5 ± 2.1	
3	21 Apr	Water	25	0	0.0	
3	21 Apr	Water	50	4	3.0 ± 3.0	
3	8 May	Sediment	1	2	11 ± 16	2.7 ± 3.9
3	8 May	Sediment	5	2	12 ± 17	2.9 ± 4.1
3	15 May	Sediment	1	27	138 ± 53	20.8 ± 8.0
3	15 May	Sediment	1	21	125 ± 54	18.9 ± 8.2
3	29 May	Sediment	1	45	4164 ± 1241	899.4 ± 268.1
3	29 May	Sediment	1	6	536 ± 437	115.8 ± 94.4
3	29 May	Sediment	50	2	249 ± 353	53.8 ± 76.2
3	29 May	Sediment	100	1	80 ± 160	17.3 ± 34.6
4	12 Jun	Sediment	5	3	285 ± 329	59.5 ± 68.7
4	12 Jun	Sediment	25	13	1533 ± 850	313.5 ± 173.8
4	12 Jun	Sediment	50	8	935 ± 661	188.4 ± 133.2

[a]The depth (m) for water sampling or sediment trap is shown.

specific ice texture but was observed both in granular and columnar ice layers in the upper 80 cm of the ice column (Figure 5a).

The brine volume fraction is a consequence of ice temperature and bulk salinity and is an indicator of ice porosity and therefore permeability, where 5% has been proposed as a percolation threshold for columnar sea ice [*Golden et al.*, 1998, 2007]. In SYI the brine volume fraction was below 5% down to 80 cm below the surface and increased below this (Figure 4d). Thus, it seems that algae were trapped in the upper layer of the ice column during winter and apparently throughout spring until the end of May. In FYI the brine volume fraction was above 5% throughout the ice column, except near the top of the core in March when the temperature was lowest (Figures 4e and 4h). Interestingly, at this time there was a minor algal maximum layer in the top of the ice (Figure 6a). This indicates that low porosity due to low temperature and/or low salinity is a mechanism that locks the algae in the brine channels in the upper part of the ice, and this is more prevalent in SYI due to the lower salinity at the top as result of desalination in summer (Figures 4b and 4f).

On Floe 4, in early June, the brine volume fraction of the FYI was >10% throughout the ice due to the elevated temperature and high salinity. This made it possible for a relatively high amount of colonial *N. frigida* to be present throughout the ice (Figure 7). If this floe had been further north in late summer or autumn at freezeup, this FYI would have formed SYI with an algal layer in the upper ice. We propose that this was the mechanism that trapped *N. frigida* and other algae in the upper part of the SYI we observed. The lower part of MYI (SYI in our case) is new ice formed during the winter [cf. *Granskog et al.*, 2017]. The reason that the algal abundance is lower in the lower part of the ice could be that the concentration of *N. frigida* in the water column was low during winter according to our counts (Table 1) and that the salinity and temperature is higher there throughout the winter, and thus, this part also has porosity above the percolation limit, allowing algae to exit the ice.

Chl *a* and algal counts were correlated in the SYI ($r = 0.61$, $p < 0.01$), and the Chl *a* to cell ratio was in the range reported for living microalgae [*Brotas et al.*, 2013]. The low amount of pigment degradation products on 22 April and 21 May suggests that the algae in the upper ice were viable. In addition, the pigment composition throughout the SYI cores for those dates was similar and showed a Chl *a* to fucoxanthin ratio characteristic for living diatoms [*Llewellyn and Gibb*, 2000]. This indicates that the cells in the upper ice had functional

photosynthetic pigments in April and had survived during the winter locked up by low porosity. It has been shown that diatoms can maintain their functional photosynthetic pigments during prolonged darkness [*Murphy and Cowles*, 1997]. To our knowledge, *N. frigidia* does not form resting spores. Instead, it seems that this diatom survives by lowering its metabolism to almost zero during the winter months [*Aletsee and Jahnke*, 1992; *Zhang et al*., 1995]. In addition, it may excrete exopolymeric substances that act as cryoprotectants against ice crystal formation and buffer against the high salinity of the brine [*Krembs et al*., 2002].

Werner et al. [2007] found an upper maximum in MYI north of Svalbard with similar abundance and algae composition to what we found in this study. *Gradinger* [1999] studied a large number of cores from thick pack ice, presumably SYI, in the central Arctic and showed many examples of upper ice algal abundance maxima with flagellates and pennate diatoms as the dominating algae. The algae were not identified to species, but the pennate diatoms were mainly in the size range 20–60 μm, which is within the size range reported for *N. frigida* [*Medlin and Hasle*, 1990]. Thus, it seems that an abundance maximum of *N. frigida* in the upper ice is a common phenomenon in MYI.

4.2. Timing of the Bottom Ice Bloom of *Nitzschia frigida* in Different Ice Types

We observed a 150-fold increase in the algal abundance in the bottom 10 cm of SYI, FYI, and YI from mid-May (Figures 5, 6, and 8). Chl *a* standing stocks in all ice types increased from initially <1 to 2.5–3 mg Chl *a* m^{-2} (not shown). The peak ice algal standing stocks we observed fall in the lower range of previously observed ice algal blooms (1–120 mg Chl *a* m^{-2}) but are typical for the region north of Svalbard [*Leu et al*., 2015]. The pennate sea ice diatom *N. frigida* was the dominant bloom species in all ice types (Figures 5, 6, and 8). In SYI and FYI the bloom reached the peak abundance on 21–23 May (Figures 5 and 6), whereas in YI approximately the same abundance was reached on 29 May (Figure 8), i.e., 1 week delayed compared with the thick ice.

The growth rate of *N. frigida* has been determined at different brine temperature and salinity and irradiance levels by *Aletsee and Jahnke* [1992]. They found that the maximum growth rate of 0.25 d^{-1} at a scalar irradiance >7 μmol photons m^{-2} s^{-1} was reached at -4°C or higher, which corresponds to a brine salinity of 73 or lower. Growth rate of *N. frigida* at different irradiance levels in irradiance-acclimated cultures at -2 to 0°C and a salinity of 34 was 0.2 d^{-1} at 10 μmol photons m^{-2} s^{-1} and the maximum growth rate was 0.23 d^{-1} at >25 μmol photons m^{-2} s^{-1} [*Juhl and Krembs*, 2010]. According to this, the temperature and salinity was always optimal for growth at the bottom of the ice during this study. Nutrients (nitrate, phosphate, and silicic acid) were all in surplus in the water below the ice until after 25 May, whereas in the ice silicic acid was always below the detection limit and nitrate became reduced to below detection during May (Figure S1). Not only uptake by algae but also brine drainage could have caused the reduction in nutrients in the ice. However, only nitrate but not phosphate decreased, suggesting that algal uptake might have been the main cause. According to *Nishi and Tabeta* [2005], a convective influx of nutrients from the water to the ice is possible during both formation and melting of sea ice. Thus, it is likely that the algae at the bottom part of the ice could exploit nutrients from the water during the bloom.

Irradiance therefore stands out as a likely growth-limiting factor. The irradiance was influenced by snow thickness and therefore very different under the different ice types (Figure 3a). Based on the under-ice irradiance, we would expect continuously maximal growth rate in YI (~0.25 d^{-1}), lower but possibly close to maximal growth during midday in FYI and around 0.07 d^{-1} in SYI according to the growth versus irradiance curves by *Juhl and Krembs* [2010]. Then, everything else being equal, the bloom should develop fastest in YI, followed by FYI and last in SYI. Contrary to this, according to our cell counts, a peak in *N. frigida* abundance of similar magnitude was reached at the same time around 21–23 May in both SYI and FYI (Figures 5 and 6) and 1 week later in YI (Figure 8).

Not only growth rate but also the initial abundance of *N. frigida* affects the time needed to reach a certain abundance. On 22 April, there were 1.2×10^3 cells L^{-1} in the bottom 10 cm of SYI. An exponential curve fit to the counts from the bottom of the SYI from 22 April and 14 and 21 May indicated an apparent growth rate of 0.16 d^{-1}. This was lower than the reported maximal growth rate for *N. frigida* [*Aletsee and Jahnke*, 1992; cf. *Juhl and Krembs*, 2010] but still higher than would be expected based on the very low irradiance. From the initial concentration of pennate diatoms, mainly *N. frigida*, of 1.4×10^3 cells L^{-1} in the bottom 10 cm of FYI in March to the maximum on 23 May the apparent growth rate was 0.10 d^{-1}, so apparently, the 10 times higher irradiance below FYI (Figure 3a) was not enough to give a higher growth rate. In YI the apparent

growth rate for *N. frigida* based on the average cell counts from the five sites was around 1 d^{-1} between 14 and 22 May, which is far above the maximal growth rate found for this species. Between 22 and 29 May it was 0.23 d^{-1}, i.e., the maximum. This together with the 1 week delay of the bloom in the YI compared with SYI and FYI suggests that *N. frigida* in the YI was supplied from the surrounding bloom in the SYI and FYI in addition to local growth.

No *N. frigida* cells were observed in YI before 22 May even though it started to form on 26 April [*Kauko et al.*, 2017], except 200 cells L^{-1} in one of the five cores on 14 May (Figure 8). To have a first idea of the possible, theoretical recruitment from the water to the ice, we made a rough estimate based on the following assumptions: *N. frigida* cells present in the mixed layer depth are all potential recruits, and when they encounter the ice, they stick to it. Then we estimated the time it takes for the water column to mix completely across the mixed layer depth, based on measured vertical diffusivity: Mixing Time (s) = (MixLayerDepth (m))^2/ Diffusivity (m^2 s^{-1}). Dividing the number of cells present in the water column (standing stock) by the mixing time yields an estimate of the time it takes for all the algae to encounter the ice and, potentially, recruit. We used measured mixed layer depth and average diffusivity across the mixed layer with 1 m vertical resolution [*Meyer et al.*, 2016]. The estimate is for the period 20 April to 10 May, i.e., before the peak of the ice algal bloom. We set the abundance of *N. frigida* to 1 cell L^{-1}, in line with our counts (Table 1). The resulting recruitment rate was in the range 3–2500 cells dm^{-2} d^{-1}, with average and median of 238 and 58 cells dm^{-2} d^{-1}, respectively. According to this, we should observe some *N. frigida* cells in the YI after 2–3 weeks. Since this was not observed, the reason might be that our assumption that every cell sticks to the ice is wrong, and this might be because most of the cells in the water in winter are not viable. From 8 May and later *N. frigida* cells were observed in increasing numbers in the sediment traps below the ice (Table 1), indicating an increasing amount of detached cells as the bloom developed in SYI and FYI. Since the older ice and the YI were just a few hundred meters apart, it is probable that cells could spread to the YI. These cells were likely to be living, and even parts of colonies, thus speeding up the seeding efficiency.

All samples from SYI and FYI on Floe 3 were taken from the same respective sampling location, with all cores from each site taken within a 10 m radius, approximately. Therefore, we followed the time development of the same patch of ice, and the algal abundance profiles in the upper ice remained similar, whereas the abundance at the bottom increased markedly due to the formation of arborescent colonies of *Nitzschia frigida* (Figure 1), characteristic for growing cells [*Medlin and Hasle*, 1990]. In the YI we sampled five sites 25 m apart from each other [*Kauko et al.*, 2017] and can assess the spatial versus temporal variability. According to the ANOSIM test, the similarity in algal composition was significantly higher between the replicate samples from the same day than between days ($p < 0.013$), i.e., temporal variation was higher than spatial variation in both the bottom 10 cm of the YI and in the top part. The FYI on Floe 4 in June showed a different profile of algal composition, with colonial *N. frigida* through the entire ice. This ice had a porosity above 10% through the entire ice (Figure 4h), which apparently enabled the existence of living colonies inside. At two of the sites we found no abundance maximum at the bottom (Figure 7). Floe 4 was entering warmer water (Figure 3b), and we observed rapid melting of the bottom of the ice [*Rösel et al.*, 2016], which probably detached algae from the ice water interface. These common features of the cores from Floe 4 are characteristic for summer sea ice with high porosity and melting of the bottom.

Other factors that may affect the observed biomass development in the ice are loss through brine drainage and predation on the ice algae. *Gradinger et al.* [1991] observed a loss of ice algae due to flushing of the ice by gravity drainage during an increase in air and ice temperature. We did not observe brine drainage events with major loss of algae from any of the ice types. In our arguments about algal growth, we implicitly assume constant and equal loss rate in all ice types. We cannot rule out that variation in predation pressure under different types of ice contributed to the differences in the timing of the algal bloom, but it has been found previously that predation has a weak impact on the abundance of ice algae and especially *N. frigida* [*Werner*, 1997; *Michel et al.*, 2002]. In our pigment analysis from SYI we found phaeophorbide, which is an indicator of grazing, only in one segment in the upper part of the 21 May core, i.e., not in the bottom of the ice.

4.3. A Proposed *Nitzschia frigida* Seed Repository in the Upper Part of Multiyear Ice

Based on our observations, we propose that SYI and older multiyear ice (MYI) serve as a seeding stock repository for *N. frigida*. The seeds are not strictly seeds but vegetative cells that survive through the winter inside the sea ice. Above we outlined a mechanism whereby seasonal changes in sea ice porosity make it possible

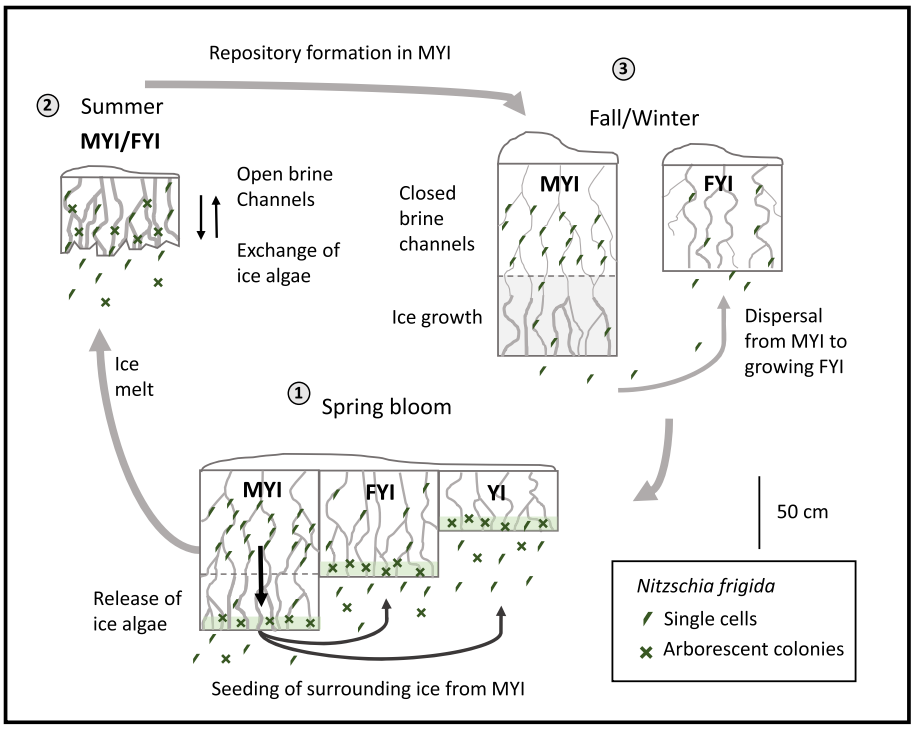

Figure 9. Conceptual scheme of a proposed mechanism in which a seed stock repository of *Nitzschia frigida* is formed in the upper part of multiyear ice (MYI). (1) As the MYI warms up in spring the porosity increases and *N. frigida* in the upper MYI can move to the bottom of the ice and initiate a sub-ice bloom. Cells can disperse from the bottom bloom in MYI to surrounding first year ice (FYI) and young ice (YI) and seed blooms there. (2) In summer when the porosity of sea ice is at maximum *N. frigida* colonies can be found inside of the ice, which could be algae detached from the bottom due to melting entering the ice or also algae growing inside of the ice. (3) In fall and winter ice that survived the melting season and became MYI cools down because of decreasing air temperature, and the brine channels close in the upper part. In this way, the algae are trapped for the winter, and a seed repository has been formed. The lower part of the MYI will be warmer because of the higher temperature in the seawater below, and therefore, the porosity is higher there. This may allow some algae to escape from the MYI also during winter and could possibly seed the surrounding younger ice continuously.

for *N. frigida* cells to enter FYI, SYI, or MYI in summer and autumn and subsequently overwinter in the upper part of the ice (Figure 9). Although we do not have direct observational evidence of it, it is likely that cells can move or be passively moved down to the bottom of the ice as the temperature, and therefore also porosity, gradually increases in spring. *Nitzchia frigida* is a raphid pennate diatom [*Medlin and Hasle*, 1990] and able to glide on surfaces like most pennates [*Wetherbee et al.*, 1998]. It is therefore likely that *N. frigida* can actively move inside brine channels. It has been demonstrated that a community of unidentified pennate sea ice diatoms was able to reposition themselves inside the ice [*Aumack et al.*, 2014]. Another possible mechanism is passive transport during brine drainage events as discussed above. Even in winter, some cells may travel down to the bottom of the ice as the seawater maintains a higher salinity and temperature at the lower part of the ice, and therefore, porosity is above the percolation threshold of about 5% brine volume fraction. From the bottom of the ice cells can disperse to surrounding ice through the under-ice water (Figure 9).

There have been some studies that concluded that the ice algal bloom inoculum could have been seeded from surrounding ice, without specifying which type of ice. *Syvertsen* [1991] proposed that ice algae are "combed" or "sieved" from the water column by platelet ice crystals at the underside of the growing ice in the Barents Sea and thus become concentrated during the winter to produce an inoculum for the spring bloom. He suggested that the algae came from ice farther north in the Barents Sea. *Niemi et al.* [2011] suggested that surrounding older ice might be the source of ice algae for FYI forming during winter. They observed cell abundances in the bottom part in the same order of magnitude as our prebloom counts. In shallow areas the sediments can serve as the seed repository for *N. frigida*. The common occurrence of this

species in, e.g., the Baltic Sea and the Hudson Bay [*Haecky et al*., 1998; *Michel et al*., 1993], which are ice free during summer, confirms this. However, this is unlikely in ice forming over the deep Arctic basins.

A transition in the sea ice regime was observed over the last decades, and ice-free summers could possibly be a reality within this century [*Stroeve et al*., 2012; *Overland and Wang*, 2013]. This means that there will be practically no SYI or MYI left in the Arctic Ocean. According to our concept that *N. frigida* needs the seed repository in SYI or MYI to maintain a sufficiently large inoculum to dominate the spring ice algal bloom in pack ice, it may, under the new ice regime with mainly FYI, become outcompeted by species that are commonly found in ice but are able to maintain populations in the water column, e.g., *Fragilariopsis cylindrus* [*von Quillfeldt*, 2004]. *F. cylindrus* is often found to be a prominent component of the Antarctic FYI regime [e.g., *Riaux-Gobin et al*., 2011]. *Melnikov et al*. [2002] concluded that changes in the physical-chemical properties of sea ice due to increased melting had changed the sea ice algae assemblage to one with less pennate diatoms like *N. frigida*, when comparing their data from pack ice in 1998 with data from the 1970s. The decrease in *N. frigida* concentrations may have consequences for the ice-associated food web, in particular for consumers that are specifically adapted to graze on bottom ice algal blooms [e.g., *Søreide et al*., 2010]. Furthermore, our results highlight the important role of seeding and inoculum size in ice algal bloom formation.

Acknowledgments

We thank the anonymous reviewers and the Editors for constructive comments. We are indebted to the captains and crew of R/V *Lance*. This study was supported by the Centre of Ice, Climate and Ecosystems at the Norwegian Polar Institute through the N-ICE project. L.M. O., H.M.K., P.A., P.D., M.A.G., S.R.L., and C.J.M. were funded by the Research Council of Norway project Boom or Bust (244646). S.R.L. was funded by the Investment in Science Fund at WHOI, USA. C.J.M. was funded by Natural Sciences and Engineering Research Council of Canada (NSERC) Discovery Grant, Canada Foundation for Innovation. M.A.G., T.T., A.K.P., and S.R.H. were funded by the Research Council of Norway project STASIS (221961).The Polish-Norwegian Research Program operated by the National Centre for Research and Development under the Norwegian Financial Mechanism 2009–2014 in the frame of project contract Pol-Nor/197511/40/2013, CDOM-HEAT, supported M.A.G., A.K.P., and S.R.H. P.A., M.F.M., and C.J.M. were supported by the Program Arktis 2030 funded by the Norwegian Ministry of Foreign Affairs and Ministry of Climate and Environment, Norway (project ID Arctic). We thank Max König for creating the map and Gunnar Spreen for help with ice floe backtracking. The following data sets were used in this study and are publicly available at the Norwegian Polar Data Centre (https://data.npolar.no): N-ICE 2015 sea ice biogeochemistry [*Assmy et al*., 2017]; N-ICE 2015 water column biogeochemistry [*Assmy et al*., 2016]; N-ICE 2015 ice core physics, temperature, salinity, and density [*Gerland et al*., 2017]; N-ICE 2015 surface meteorology [*Hudson et al*., 2015]; N-ICE 2015 ocean microstructure profiles [*Meyer et al*., 2016]; N-ICE 2015 phytoplankton and ice algae taxonomy and abundance [*Olsen et al*., 2017]; N-ICE 2015 total snow and ice thickness data from EM31 [*Rösel et al*., 2016]; and N-ICE 2015 surface and under-ice spectral shortwave radiation data [*Taskjelle et al*., 2016]. See reference list for the DOI of each data set.

References

Aletsee, L., and J. Jahnke (1992), Growth and productivity of the psychrophilic marine diatoms *Thalassiosira Antarctica* Comber and *Nitzschia frigida* Grunow in batch cultures at temperatures below the freezing point of sea water, *Polar Biol.*, *11*, 643–647.

Assmy, P., et al. (2016), N-ICE2015 water column biogeochemistry, Norwegian Polar Institute, doi:10.21334/npolar.2016.3ebb7f64.

Assmy, P., et al. (2017), N-ICE2015 sea ice biogeochemistry, Norwegian Polar Institute, doi:10.21334/npolar.2017.d3e93b31.

Aumack, C., A. R. Juhl, and C. Krembs (2014), Diatom vertical migration within land-fast Arctic sea ice, *J. Mar. Syst.*, *139*, 496–504.

Brotas, V., et al. (2013), Deriving phytoplankton size classes from satellite data: Validation along a trophic gradient in the eastern Atlantic Ocean, *Remote Sens. Environ.*, *134*, 66–77, doi:10.1016/j.rse.2013.02.013.

Clarke, K. R. (1993), Non-parametric multivariate analyses of changes in community structure, *Aust. J. Ecol.*, *18*, 117–143.

Cohen, L., S. Hudson, V. P. Walden, R. A. Graham, and M. A. Granskog, (2017) Meteorological conditions in a thinner Arctic sea ice regime from winter through spring during the Norwegian Young Sea Ice expedition (N-ICE2015), *J. Geophys. Res. Atmos.*, doi:10.1002/2016JD026034.

Cox, G. F. N., and W. F. Weeks (1986), Changes in the salinity and porosity of sea-ice samples during shipping and storage, *J. Glaciol.*, *32*(112), 371–375.

Edler, L., and M. Elbrächter (2010), The Utermöhl method for quantitative phytoplankton analysis, in *Microscopic and Molecular Methods for Quantitative Phytoplankton Analysis*, *Intergovernmental Oceanographic Commission of UNESCO (2010)*, edited by B. Karlson, C. Cusack, and E. Bresnan, pp. 13–20, UNESCO, Paris.

Fragoso, G. M., A. J. Poulton, I. M. Yashayaev, E. J. H. Head, and D. A. Purdie (2016), Spring phytoplankton communities of the Labrador Sea (200–2014): Pigment signatures, photophysiology and elemental ratios, *Biogeosci. Discuss.*, doi:10.5194/bg-2016-295.

Gerland, S., M. A. Granskog, J. King, and A. Rösel (2017), N-ICE2015 ice core physics: Temperature, salinity and density, Norwegian Polar Institute, doi:10.21334/npolar.2017.c3db82e3.

Girard-Ardhuin, F., and R. Ezraty (2012), Enhanced Arctic sea ice drift estimation merging radiometer and scatterometer data, *IEEE Trans. Geosci. Remote Sens.*, *50*, 2639–2648.

Golden, K. M., S. F. Ackley, and V. I. Lytle (1998), The percolation phase transition in sea ice, *Science*, *282*, 2238–2241.

Golden, K. M., H. Eicken, A. L. Heaton, J. Miner, D. J. Pringle, and J. Zhu (2007), Thermal evolution of permeability and microstructure in sea ice, *Geophys. Res. Lett.*, *34*, L16501, doi:10.1029/2007GL030447.

Gradinger, R., M. Spindler, and D. Henschel (1991), Development of Arctic sea-ice organisms under graded snow cover, *Polar Res.*, *10*(1), 295–308, doi:10.3402/polar.v10i1.6748.

Gradinger, R. (1999), Vertical fine structure of the biomass and composition of algal communities in Arctic pack ice, *Mar. Biol.*, *133*, 745–754.

Granskog, M., H. Kaartokallio, H. Kuosa, D. N. Thomas, and J. Vainio (2006), Sea ice in the Baltic Sea—A review, *Estuarine Coastal Shelf. Sci.*, *70*, 145–160.

Granskog, M. A., et al. (2016), Arctic research on thin ice: Consequences of Arctic sea ice loss, *Eos Trans. AGU*, *97*, 22–26, doi:10.1029/2016EO044097.

Granskog, M., A. Rösel, P. Dodd, D. Divine, S. Gerland, T. Martma, and M. Leng (2017), Snow contribution to first-year and second-year Arctic sea ice mass balance north of Svalbard, *J. Geophys. Res. Oceans*, *122*, 2539–2549, doi:10.1002/2016JC012398.

Haecky, P., S. Jonsson, and A. Andersson (1998), Influence of sea ice on the composition of the spring phytoplankton bloom in the northern Baltic Sea, *Polar Biol.*, *20*, 1, doi:10.1007/s003000050270.

Head, E. J. H., and L. R. Harris (1992), Chlorophyll and carotenoid transformation and destruction by *Calanus* spp. grazing on diatoms, *Mar. Ecol. Prog. Ser.*, *86*, 229–238, doi:10.3354/meps086229.

Holm-Hansen, O., and B. Riemann (1978), Chlorophyll *a* determination: Improvements in methodology, *Oikos*, *30*, 438–447.

Horner, R. (1985), *Sea Ice Biota*, CRC Press, Boca Raton, Fla.

Hudson, S. R., L. Cohen, and V. Walden (2015), N-ICE2015 surface meteorology, Norwegian Polar Institute, doi:10.21334/npolar.2015.056a61d1.

Itkin, P., G. Spreen, B. Cheng, M. Doble, F. Girard-Ardhuin, J. Haapala, N. Hughes, L. Kaleschke, M. Nicolaus, and J. Wilkinson (2017), Thin ICE and storms: Sea ice deformation from buoy arrays deployed during N-ICE2015, *J. Geophys. Res. Oceans*, doi:10.1002/2016JC012403.

Jakobsson, M., et al. (2012), The International Bathymetric Chart of the Arctic Ocean (IBCAO) Version 3.0, *Geophys. Res. Lett.*, *39*, L12609, doi:10.1029/2012GL052219.

Jeffrey, S. W., and M. Vesk (1997), *Phytoplankton Pigments in Oceanography: Guideline to Modern Methods*, *Unesco Monogr. Oceanogr. Methods*, edited by S. W. Jeffrey, R. F. C. Mantoura, and S. W. Wright, pp. 37–84, UNESCO, Paris.

Juhl, A. R., and C. Krembs (2010), Effects of snow removal and algal photoacclimation on growth and export of ice algae, *Polar Biol.*, *33*(8), 1057–1065, doi:10.1007/s00300-010-0784-1.
Kauko, H. M., et al. (2017), Windows in Arctic sea ice: Light transmission and ice algal optical properties in a refrozen lead, *J. Geophys. Res. Biogeosci.*, doi:10.1002/2016JG003626.
Krell, A., B. Beszteri, G. Dieckmann, G. Glöckner, K. Valentin, and T. Mock (2008), A new class of ice-binding proteins discovered in a salt-stress-induced cDNA library of the psychrophilic diatom *Fragilariopsis cylindrus* (Bacillariophyceae), *Eur. J. Phycol.*, *43*(4), 423–433, doi:10.1080/09670260802348615.
Krembs, C., H. Eicken, K. Junge, and J. W. Deming (2002), High concentrations of exopolymeric substances in Arctic winter sea ice: Implications for the polar ocean carbon cycle and cryoprotection of diatoms, *Deep Sea Res., Part I*, *49*, 2163–2181.
Laney, S. R., and H. M. Sosik (2014), Phytoplankton assemblage structure in and around a massive under-ice bloom in the Chukchi Sea, *Deep Sea Res., Part II*, *105*, 30–41.
Lange, M. A. (1988), Basic properties of Antarctic sea ice revealed by textural analysis of ice cores, *Ann. Glaciol.*, *10*, 95–101.
Leu, E., C. J. Mundy, P. Assmy, K. Campbell, T. M. Gabrielsen, M. Gosselin, T. Juul-Pedersen, and R. Gradinger (2015), Arctic spring awakening—Steering principles behind the phenology of vernal ice algal blooms, *Prog. Oceanogr.*, *139*, 151–170.
Llewellyn, C. A., and S. W. Gibb (2000), Intra-class variability in the carbon, pigment and biomineral content of prymnesiophytes and diatoms, *Mar. Ecol. Prog. Ser.*, *193*, 33–44, doi:10.3354/meps193033.
Light, B., T. C. Grenfell, and D. K. Perovich (2008), Transmission and absorption of solar radiation by Arctic sea ice during the melt season, *J. Geophys. Res.*, *113*, C03023, doi:10.1029/2006JC003977.
Lundholm, N., and G. R. Hasle (2008), Are *Fragilariopsis cylindrus* and *Fragilariopsis nana* bipolar diatoms?—Morphological and molecular analyses of two sympatric species, *Nova Hedwig. Beih.*, *133*, 231–250.
Lyon, B. R., and T. Mock (2014), Polar microalgae: New approaches towards understanding adaptations to an extreme and changing environment, *Biology*, *3*, 56–80.
Medlin, L., and G. Hasle (1990), Some *Nitzschia* and related diatom species from fast ice samples in the Arctic and Antarctic, *Polar Biol.*, *10*, 451–479.
Melnikov, I. A., E. G. Kolosova, H. E. Welch, and L. S. Zhitina (2002), Sea ice biological communities and nutrient dynamics in the Canada Basin of the Arctic Ocean, *Deep Sea Res., Part I*, *49*, 1623–1649.
Meyer, A., et al. (2016), N-ICE2015 ocean microstructure profiles (MSS90L), Norwegian Polar Institute, doi:10.21334/npolar.2016.774bf6ab.
Meyer, A., et al. (2017), Winter to summer oceanographic observations in the Arctic Ocean north of Svalbard, *J. Geophys. Res. Oceans*, doi:10.1002/2016JC012391.
Michel, C., L. Legendre, J. C. Therriault, S. Demers, and T. Vandevelde (1993), Springtime coupling between ice algal and phytoplankton assemblages in southeastern Hudson Bay, Canadian Arctic, *Polar Biol.*, *13*, 441–449.
Michel, C., T. G. Nielsen, C. Nozais, and M. Gosselin (2002), Significance of sedimentation and grazing by ice micro- and meiofauna for carbon cycling in annual sea ice (northern Baffin Bay), *Aquat. Microb. Ecol.*, *30*, 57–68.
Montresor, M., C. Lovejoy, L. Orsini, G. Procacci, and S. Roy (2003), Bipolar distribution of the cyst-forming dinoflagellate Polarella glacialis, *Polar Biol.*, *26*, 186, doi:10.1007/s00300-002-0473-9.
Murphy, A. M., and T. J. Cowles (1997), Effects of darkness on multi-excitation in vivo fluorescence and survival in a marine diatom, *Limnol. Oceanogr.*, *42*, 1444–1453.
Niemi, A., C. Michel, K. Hille, and M. Poulin (2011), Protist assemblages in winter sea ice: Setting the stage for the spring ice algal bloom, *Polar Biol.*, *34*(12), 1803–1817.
Nishi, Y., and S. Tabeta (2005), Analysis of the contribution of ice algae to the ice-covered ecosystem in Lake Saroma by means of a coupled ice–ocean ecosystem model, *J. Mar. Syst.*, *55*, 249–270.
Olsen, L. M., et al. (2017), N-ICE2015 phytoplankton and ice algae taxonomy and abundance, Norwegian Polar Institute, doi:10.21334/npolar.2017.dc61cb24.
Olson, R. J., and H. M. Sosik (2007), A submersible imaging-in-flow instrument to analyze nano-and microplankton: Imaging FlowCytobot, *Limnol. Oceanogr. Methods*, *5*, 195–203.
Overland, J. E., and M. Wang (2013), When will the summer Arctic be nearly sea ice free?, *Geophys. Res. Lett.*, *40*, 2097–2101, doi:10.1002/grl.50316.
Owens, T. G., and P. G. Falkowski (1982), Enzymatic degradation of chlorophyll *a* by marine phytoplankton in vitro, *Phytochemistry*, *21*, 979–984, doi:10.1016/S0031-9422(00)82401-2.
Petrich, C., and H. Eicken (2010), Growth, structure and properties of sea ice, in *Sea Ice*, 2nd ed., edited by D. N. Thomas and G. S. Dieckmann, pp. 23–77, Wiley-Blackwell, Oxford, U. K. doi:10.1002/9781444317145.ch2.
Poulin, M., N. Daugbjerg, R. Gradinger, L. Ilyash, T. Ratkova, and C. von Quillfeldt (2011), The pan-Arctic biodiversity of marine pelagic and sea-ice unicellular eukaryotes: A first-attempt assessment, *Mar. Biodivers.*, *41*, 13–28.
R Development Core Team (2008), *R: A Language and Environment for Statistical Computing*, R Foundation for Statistical Computing, Vienna. [Available at www.R-project.org.]
Ratkova, T. N., and P. Wassman (2005), Sea ice algae in the White and Barents seas: Composition and origin, *Polar Res.*, *24*, 95–110.
Riaux-Gobin, C., M. Poulin, G. Dieckmann, C. Labrune, and G. Vetion (2011), Spring phytoplankton onset after the ice break-up and sea-ice signature (Adelie Land, East Antarctica), *Polar Res.*, *30*, 5910, doi:10.3402/polar.v30i0.5910.
Rigor, I. G., R. L. Colony, and S. Martin (2000), Variations in surface air temperature observations in the Arctic, 1979–97, *J. Clim.*, *13*, 896–914.
Rigor, I. G., and J. M. Wallace (2004), Variations in the age of Arctic sea-ice and summer sea-ice extent, *Geophys. Res. Lett.*, *31*, L09401, doi:10.1029/2004GL019492.
Rintala, J.-M., J. Piiparinen, J. Blomster, M. Majaneva, S. Muller, J. Uusikivi, and R. Autio (2014), Fast direct melting of brackish sea-ice samples results in biologically more accurate results than slow buffered melting, *Polar Biol.*, *37*, 1811–1822.
Rösel, A., et al. (2016), N-ICE2015 total (snow and ice) thickness data from EM31, doi:10.21334/npolar.2016.70352512.
Sinha, N. K. (1977), Technique for studying structure of sea ice, *J. Glaciol.*, *18*, 315–323.
Stoecker, D. K., D. E. Gustafson, M. M. D. Black, and C. T. Baier (1998), Population dynamics of microalgae in the upper land-fast sea ice at a snow-free location, *J. Phycol.*, *34*, 60–69.
Stroeve, J. C., M. C. Serreze, M. M. Holland, J. E. Kay, J. Malanik, and A. P. Barrett (2012), The Arctic's rapidly shrinking sea ice cover: A research synthesis, *Clim. Change*, *110*, 1005–1027.
Syvertsen, E. E. (1991), Ice algae in the Barents Sea: Types of assemblages, origin, fate and role in the ice-edge phytoplankton bloom, *Polar Res.*, *10*, 277–288.
Søreide, J. E., E. Leu, J. Berge, M. Graeve, and S. Falk-Petersen (2010), Timing of blooms, algal food quality and *Calanus glacialis* reproduction and growth in a changing Arctic, *Global Change Biol.*, *16*, 3154–3163, doi:10.1111/j.1365-2486.2010.02175.x.

Taskjelle, T., S. R. Hudson, A. Pavlov, and M. A. Granskog (2016), N-ICE2015 surface and under-ice spectral shortwave radiation data, Norwegian Polar Inst., doi:10.21334/npolar.2016.9089792e.
Timco, G. W., and R. M. W. Frederking (1996), A review of sea ice density, *Cold Regions Sci. Tehnol.*, *24*, 1–6.
Thomas, D. N., and G. S. Dieckmann (2002), Antarctic Sea ice—A habitat for extremophiles, *Science*, *295*, 641–644.
Tran, S., B. Bonsang, V. Gros, I. Peeken, R. Sarda-Esteve, A. Berhardt, and S. Belvisio (2013), A survey of carbon monoxide and non-methane hydrocarbons in the Arctic Ocean during summer 2010, *Biogeosciences*, *10*, 1909–1935.
von Quillfeldt, C. H. (2001), Identification of some easily confused common diatom species in arctic spring blooms, *Botanica Marina*, *44*(4), 375–389, doi:10.1515/BOT.2001.048.
von Quillfeldt, C. H., W. G. Ambrose Jr., and L. M. Clough (2003), High number of diatom species in first-year ice from the Chukchi Sea, *Polar Biol.*, *26*(12), 806–818.
von Quillfeldt, C. H. (2004), The diatom *Fragilariopsis cylindrus* and its potential as an indicator species for cold water rather than for sea ice, *Vie Milieu*, *54*, 137–143.
von Quillfeldt, C. H., E. N. Hegseth, G. Johnsen, E. Sakshaug, and E. E. Syvertsen (2009), Ice algae, in *Ecosystem Barents Sea*, edited by E. Sakshaug, G. Johnsen, and K. M. Kovacs, pp. 285–302, Tapir Acad. Press, Trondheim, Norway.
Werner, I. (1997), Grazing of Arctic under-ice amphipods on sea-ice algae, *Mar. Ecol. Prog. Ser.*, *160*, 93–99.
Werner, I., J. Ikävalko, and H. Schünemann (2007), Sea-ice algae in Arctic pack ice during late winter, *Polar Biol.*, *30*, 1493–1504.
Wetherbee, R., J. L. Lind, J. Burke, and R. S. Quatran (1998), The first kiss: Establishment and control of initial adhesion by rapid diatoms, *J. Phycol.*, *34*, 9–15.
Willmes, S., and G. Heinemann (2016), Sea-ice wintertime lead frequencies and regional characteristics in the Arctic, 2003–2015, *Remote Sens.*, *8*, 4.
Zhang, Q., R. Gradinger, and M. Spindler (1995), Dark survival of marine micro algae in the high Arctic (Greenland Sea), *Polarforschung*, *65*, 111–116.